

pubs.acs.org/ac Article

Label-Free and Ultrasensitive Electrochemical DNA Biosensor Based on Urchinlike Carbon Nanotube-Gold Nanoparticle Nanoclusters

Shuo Han, Wenyan Liu,* Ming Zheng, and Risheng Wang*



Cite This: Anal. Chem. 2020, 92, 4780-4787



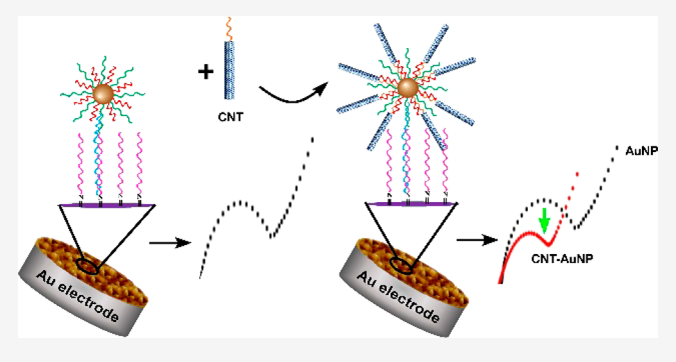
ACCESS

Metrics & More



3 Supporting Information

ABSTRACT: Nanomaterials have been extensively utilized in biosensing systems for highly sensitive and selective detection of a variety of biotargets. In this work, a facile, label-free, and ultrasensitive electrochemical DNA biosensor has been developed, based on "urchinlike" carbon nanotube-gold nanoparticle (CNT-AuNP) nanoclusters, for signal amplification. Specifically, electrochemical polymerization of dopamine (DA) was employed to modify a gold electrode for immobilization of DNA probes through the Schiff base reaction. Upon sensing the target nucleic acid, the dual-DNA (reporter and linker) functionalized AuNPs were introduced into the sensing system via DNA hybridization. Afterward, the end-modified single-wall carbon nanotubes with



DNA (SWCNT-DNA) were attached to the surface of the AuNPs through linker-DNA hybridization that formed 3D radial nanoclusters, which generated a remarkable electrochemical response. Because of the larger contact surface area and super electronic conductivity of CNT-AuNP clusters, this novel designed 3D radial nanostructure exhibits an ultrasensitive detection of DNA, with a detection limit of 5.2 fM (a linear range of from 0.1 pM to 10 nM), as well as a high selectivity that discriminates single-mismatched DNA from fully matched target DNA under optimal conditions. This biosensor, which combines the synergistic properties of both CNTs and AuNPs, represents a promising signal amplification strategy for achieving a sensitive biosensor for DNA detection and diagnostic applications.

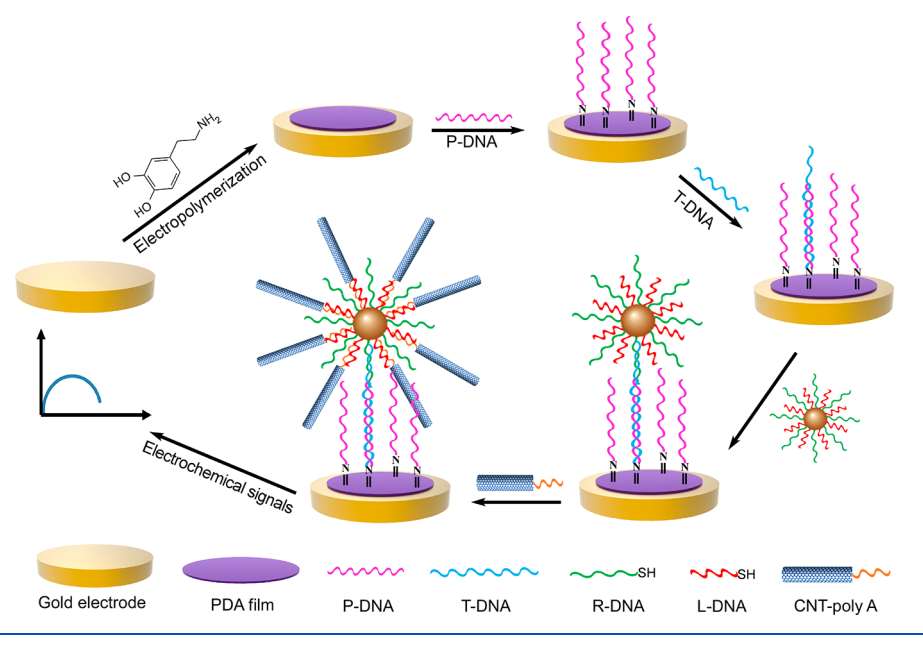
In the last two decades, DNA biosensors, based on nucleic acid hybridization, have been widely employed in many fields, ranging from molecular diagnostics, gene therapy, and environmental analysis, to food development. Among the existing DNA detection techniques, electrochemical DNA biosensors have received extensive interest because of their high sensitivity, simplicity, low-cost, and potential for miniaturization.

Detection of ultralow content of DNA in samples has also attracted tremendous research attention. Thus, in order to further improve the sensitivity and detection level of electrochemical DNA biosensing, a variety of signal amplification strategies have been reported, including rolling circle amplification (RCA), nanocomposites, catalyzed hairpin assembly (CHA), and so on. 10-15 Among them, nanocomposites that are typically constructed by combining two or more nanomaterials, have gained increasing interest because of their unique physical and chemical properties. One of the most frequently used nanomaterials for the fabrication of nanocomposites is gold nanoparticles (AuNPs). AuNPs, conjugated with different reporter molecules, such as ferrocene (Fc), 16 thionine, 17 and enzymes, 18 have been used to amplify the signal during DNA detection by taking advantage of the outstanding properties of the AuNPs, which include easy surface modification, quantized charging/discharging characteristics, electrocatalysis, and biocompatibility. 19 Apart from the AuNPs, carbon nanotubes (CNTs) are another popularly utilized candidate used in nanocomposites (e.g., horseradish peroxidase (HRP)-CNT,²⁰ Fc-CNT,²¹ alkaline phosphatase (ALP)-CNT²² conjugates, and so on) for signal amplification. This is due to their high electronic conductivity for electron transfer reactions and excellent sensitivity for monitoring chemical environmental changes around their surfaces. Recently, AuNP-CNT nanocomposites have shown great potential for advancing DNA detection because of their enhanced physical and excellent synergistic properties. For example, Ma et al. covalently attached multiwalled carbon nanotubes (MWCNTs) and AuNPs, via a layer-by-layer assembly technique on an electrode, which showed excellent reproducibility and stability for DNA detection, with a limit of 7.5 pM.²⁴ Moreover, Fayazfar et al. fabricated another biosensing platform for label-free detection of TP53 gene mutation, based on AuNPs/vertically aligned MWCNT nanocomposites, where the synergistic interactions of the

Received: August 2, 2019
Accepted: February 14, 2020
Published: February 14, 2020



Scheme 1. Schematic Illustration of the Fabrication and Detection Process of an Electrochemical DNA Biosensor



AuNPs and the vertically aligned CNTs on an electrode surface not only improved the density of the probe DNA attachment and accessibility for DNA hybridization but also enhanced the electron transfer reaction. Though much progress has been made with nanocomposite-assisted DNA sensing systems, it is still highly desirable to explore new strategies that can effectively amplify and transduce DNA hybridization signals to achieve higher sensitivity and accuracy in the electrochemical detection of nucleic acids.

In this work, we report a simple, label-free, and ultrasensitive sandwich-type electrochemical biosensor for DNA detection, based on a novel urchinlike CNT-AuNP nanoclusters serving as a signal amplifier. The unique morphology of the fabricated nanoclusters effectively facilitates the electron transfer between the electrode and hybridized clusters, therefore significantly enhancing the signal of DNA interaction. As illustrated in Scheme 1, the DNA biosensor was prepared by covalently attaching the amine-modified probe DNA (NH2-ssDNA) onto the polydopamine (PDA)-functionalized gold electrode surface through the Schiff base reactions, where the catechol functional groups of PDA coupled with amine group-modified DNA to anchor DNA probes on the interface of PDA.²⁶⁻²⁹ Upon hybridization of the probe DNA with the target DNA, the dual-DNA (reporter and linker) functionalized AuNPs were introduced into the sensing system via DNA hybridization. Afterward, the end-modified single-wall carbon nanotubes with DNA (SWCNT-DNA) were attached to the surface of the DNA-functionalized AuNPs through linker-DNA hybridization, forming three-dimensional (3D) urchinlike nanoclusters. Because of the flexibility of DNA strands, relatively large mass of AuNPs, and a large contact surface area of conjugated CNTs, the CNT-AuNP nanoclusters were positioned in close proximity of the gold electrode surface, allowing an efficient electron transfer reaction. The fabrication processes and performance of the DNA biosensor were characterized by cyclic voltammetry (CV) and electrochemical impedance spectroscopy (EIS), as well as linear sweep voltammetry (LSV).

EXPERIMENTAL SECTION

Materials and Chemicals. All synthetic DNA strands were purchased from Integrated DNA Technologies, Inc. (www.idtdna.com), and their corresponding sequences are included in Supporting Information, Table S1. Dopamine hydrochloride (DA), tris(hydroxymethyl)aminomethane (Tris), trisodium citrate, and tris(2-carboxyethyl)phosphine (TCEP) were purchased from Sigma-Aldrich. Gold nanoparticles (15 nm) were purchased from Ted Pella, Inc. 2× Saline sodium citrate (SSC) buffer (300 mM NaCl, 30 mM sodium citrate, pH 7.0) was used as a hybridization buffer, and 0.2× SSC was used as a washing buffer.

Apparatus. Electrochemical analysis was carried out on an Ivium CompactStat potnetiostat(Ivium Technologies, Netherlands) at room temperature. All experiments were conducted with a conventional three-electrode system, including a gold working electrode (WE), a Pt mesh counter electrode (CE), and a Ag/AgCl (3.0 M KCl) reference electrode (RE). Electrochemical impedance spectroscopy (EIS) was performed at a frequency that ranged from 0.1 Hz to 10 kHz. All experimental results were analyzed in terms of a Randle's equivalent circuit model. AuNPs concentrations were determined by using a UV-vis spectrophotometer (Ultrospec 9000, GE Healthcare). Atomic force microscope (AFM) images were obtained using a Nanoscope III microscope (Digital Instruments, Santa Barbara, CA), operating in a tapping mode in air, with ultrasharp 14 series (NSC 14) tips purchased from NanoWorld (www.nanoworld.com).

Functionalization of Gold Nanoparticles with Thiolated Reporter and Linker ssDNA. AuNPs (15 nm) were functionalized with a mixture of thiolated reporter and linker ssDNA (molar ratio at 50:50) by following the previously introduced methods. First, the thiolated DNA strands were reduced by TCEP in Milli-Q water with a TCEP:DNA ratio of 100:1 for 1 h, followed by filtration to remove small molecules using a G-25 column. Then, the reduced thiolated DNA was mixed with an AuNP solution and, subsequently, incubated at room temperature on a shaking mixer (Global Scientific In). After 1 h, 1× phosphate buffered saline (PBS, 100 mM NaCl,

10 mM phosphate) was added to the mixed solution, and the mixture was aged for 2 h. Next, a salt NaCl solution (2 M) was gradually added to the above solution to reach a final NaCl concentration of 0.5M, and the mixture was aged on a shaking mixer for another 12 h. Last, the DNA-coated AuNPs were centrifuged and washed three times with a 0.1 M PBS buffer (0.1 M NaCl, 10 mM phosphate) to remove unbound DNA strands. The AuNP concentration was measured by a UV—vis spectrophotometer at 520 nm.

Preparation of 3D Radial AuNP-CNT Nanocomposites. The DNA-wrapped-CNTs, containing carboxyl groups on the ends, were prepared by following previous methods.31-33 In brief, bundled SWCNTs are effectively dispersed in water by their sonication in the presence of ssDNA. Then the DNA-coated CNTs are separated into fractions with different electronic structures by ion-exchange chromatography. The prepared DNA-CNTs were first activated in a 0.2 M MES buffer, with 4 mM EDC and 10 mM sulfo-NHS, for 30 min at room temperature, followed by the addition of amine-DNA (0.5 μ M) to the CNT solution. After overnight incubation, at room temperature, the mixture went through a 100 K centrifugal filter (6,000 rpm, 3 min) to remove excess unbound DNA. Then, the DNA-end-functionalized CNTs were mixed with DNA-modified AuNPs at a volume ratio of 1:4 and, subsequently, annealed from 50 °C to room temperature overnight, to promote the formation of the 3D radial CNT-AuNP nanoclusters.

Fabrication of DNA Biosensor. The bare gold electrode (3 mm in diameter) was carefully polished to a mirrorlike finish with an aqueous solution of alumina powder (0.3 and 0.05 μ m) on a polishing cloth and sonicated for 10 min in Milli-Q water. Subsequently, the electrode was cleaned in 0.5 M sulfuric acid by applying an electric potential ranging from 0.0 to 1.5 V, until a standard cyclic peak was observed. The mirror-finish gold electrode was then dried with nitrogen and was ready for further modification. The electrochemical polymerization of dopamine (DA) on the surface of the electrode was performed by the cyclic sweep of a potential for 10 successive cycles between -0.4 V and +1.5 V, at a scan rate of 20 mV/s, in 20 mL of 1× PBS buffer (pH 6.5), containing 5.0 mM DA. The modified electrode was then washed with 1× PBS buffer and gently blown dry with compressed nitrogen.

The probe DNA (1 μ M) was immobilized on the PDA-modified electrode, via a Schiff base reaction, by dropping 10 μ L of a probe DNA solution on the electrode and incubating it at room temperature. After 12 h, the residual activated PDA film was completely blocked through ethanolamine hydrochloride (1.0 mM) treatment. The resulting DNA-modified electrode was then washed with 1× PBS to remove unbound probe DNA and stored in the immobilization buffer until further use.

Electrochemical Detection of DNA Hybridization and Signal Recording. The probe-modified electrode was incubated with target DNA (1 μ M) in a 10 mM Tris-HCl buffer (pH 7.5) for 60 min at 42 °C. The electrode was then rinsed three times with the 10 mM Tris-HCl buffer to remove nonhybridized target DNA from the electrode surface. To amplify the electrochemical signal, the target-hybridized electrode was immersed in the dual-DNA modified AuNPs solution for 60 min at 42 °C, following washing. Then, the prepared electrode was incubated with the SWCNT-DNA solution (500 nM) and cooled from 45 °C to room temperature. Thereafter, the excess was thoroughly washed

from the electrode with washing buffer to ensure that the current signal obtained was only caused by the AuNP-CNT nanoclusters hybridized with target DNA. Finally, LSV measurements were carried out in a 5.0 mM $\left[\text{Fe}(\text{CN})_6 \right]^{4-/3}$ solution containing 0.10 M KCl in a scan ranging from -0.2 V to +0.6 V.

RESULTS AND DISCUSSION

Synthesis and Characterization of 3D Urchinlike CNT-AuNP Nanoclusters. In this study, ssDNA wrapped single-walled CNTs were employed that contained carboxyl groups on both ends that were created during the cutting process. ^{31–33} By following previous methods, NH₂-ssDNA was easily attached on the ends of the CNT through amide bond formation. ³⁴ Then, CNTs were conjugated on the surface of dual-DNA (reporter and linker) functionalized AuNPs, through DNA hybridization, in which the sequence of DNA on CNTs was complementary to the reporter DNA on AuNPs. To verify the successful formation of the CNT-AuNP nanoclusters, AFM was employed to directly visualize their size and morphology. The typical AFM image of the assembled CNT-AuNP nanoclusters, as shown in Figure 1, clearly reveals

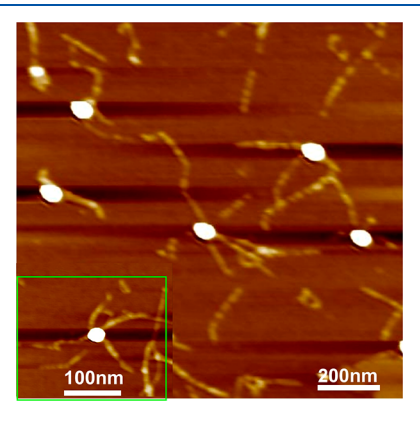


Figure 1. AFM image showing the formation of 3D urchinlike CNT-AuNP nanoclusters. Scale bar: 200 nm.

that the CNTs with a length distribution of 100-150 nm (Figure S1) could radially attach to the surface of the DNA-functionalized AuNPs (~ 15 nm core diameter), and form the targeted clusters. The statistic distribution of the number of CNT on a single AuNP shows in Figure S2. The diameter of these nanoclusters was estimated to be up to 300 nm.

Electropolymerization of Dopamine at the Surface of a Gold Electrode. Cyclic voltammetry, a powerful electrochemical technique, was used for electropolymerization of the PDA film on the surface of a gold electrode.^{35–37} Figure 2A presents the repetitive CV curves (10 cycles) obtained during electropolymerization. It can be seen that, in the first cycle, peak 1 was observed at +0.2 V, which is attributed to the oxidation of the DA. In addition, a pair of well-defined peaks (2 and 3) appeared at +0.11 V and -0.33 V, respectively, which could have resulted from the reduction of dopaminequinone (DAQ) and dopaminechrome (DAC), respectively. In subsequent potential scans, an additional peak (4) was observed at -0.23 V, which was likely because of the oxidation of leucodopaminechrome (LDAC). 38-40 It is worth noting that the peak currents of peaks 1 and 2 gradually decreased with the increased number of scans. This effect suggests that the oxidation products of DA were polymerized and

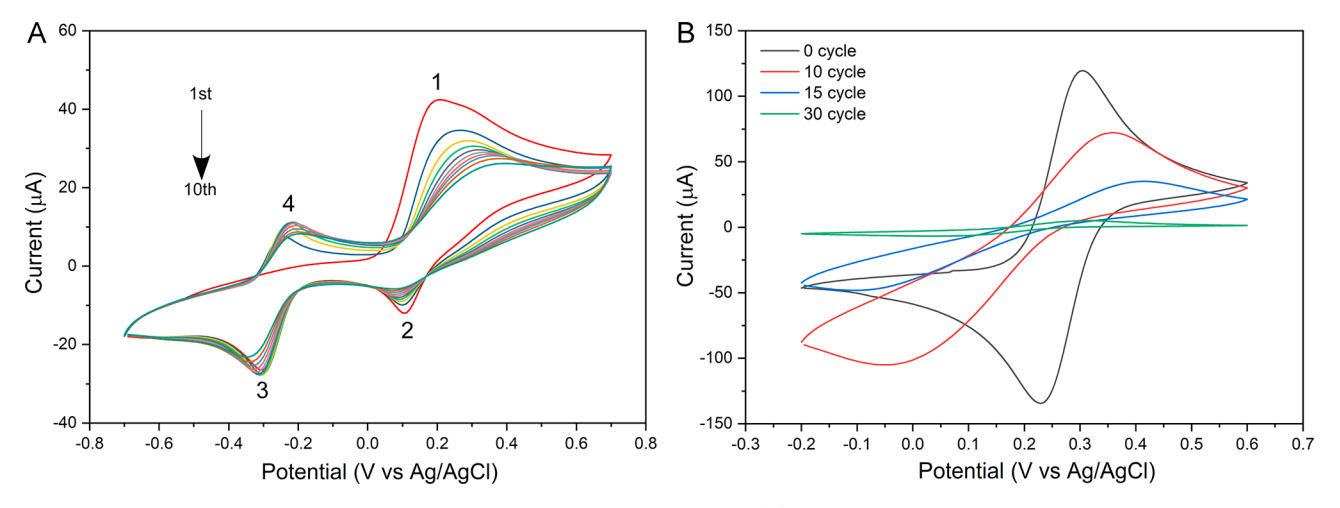


Figure 2. Electropolymerization of dopamine at the surface of a gold electrode. (A) Repetitive electrochemical polymerization of DA by cyclic voltammograms at the surface of a gold electrode. Scan rate: 100 mV/s with potential range from -0.7 V to +0.7 V; (B) Cyclic voltammograms of different voltammetric cycles of PDA-modified gold electrode containing 5 mM $[\text{Fe}(\text{CN})_6]^{3^{-4}}$ with a 50 mV/s scan rate.

successfully adsorbed onto the electrode surface, therefore, leading to the suppression of the voltammetric response. The electrochemical behavior of electrodeposited PDA film on the electrode surface was further investigated by using [Fe- $(CN)_6$]^{3-/4-} as a redox probe during CV scans.

As illustrated in Figure 2B, the bare gold exhibited a pair of well-defined, nearly reversible redox peaks with a peak potential difference of 70.5 mV. Nevertheless, with increases in the cycling number of electropolymerization, the peak currents decreased rapidly and, meanwhile, the peak-to-peak separation gradually increased. Once 30 cycles were reached, both redox peaks disappeared almost completely, indicating that a continuous and dense PDA film was coated on the gold electrode surface, which nearly blocked the electron transfer reaction of $[Fe(CN)_6]^{3-/4-}$.

Fabrication of DNA Biosensor. EIS is a highly effective method for monitoring the changes in interfacial behavior that occurs on a surface-modified electrode in each fabrication process.⁴¹ EIS data are commonly evaluated with a Nyquist plot, which includes a semicircle portion that is observed in a higher frequency region and a straight line at a low-frequency region. The diameter of the semicircle represents the electrotransfer resistance (R_{et}) , the value of which is directly dependent on the characteristics of the surface layer and, therefore, allows the monitoring of each step of electrode fabrication.42 The simplest, and most frequently used equivalent circuit for modeling the EIS experimental data is the Randles circuit which comprises the uncompensated resistance of the electrolyte (R_S) , constant phase element $(C_{\rm dl})$, the charge-transfer resistance $(R_{\rm ct})$, and the Warburg impedance $(Z_{\rm w})$. Figure 3 shows the Nyquist plots of the stepwise fabrication processes of a DNA biosensor. It is observed that the R_{ct} value had increased after electropolymerization of the PDA coating on the electrode surface, as compared with the bare gold electrode that exhibited a nearly straight line. This result indicated that the PDA film partially blocked the electron transfer between $[Fe(CN)_6]^{3-/4-}$ in the solution and the electrode surface. After the probe DNA strands were immobilized on the PDA layer of the electrode, the $R_{\rm ct}$ value obviously increased to 3500 Ω , as a result of the electrostatic repulsive force between the negatively charged DNA backbone and the $[Fe(CN)_6]^{3-/4-}$. In sequence, when

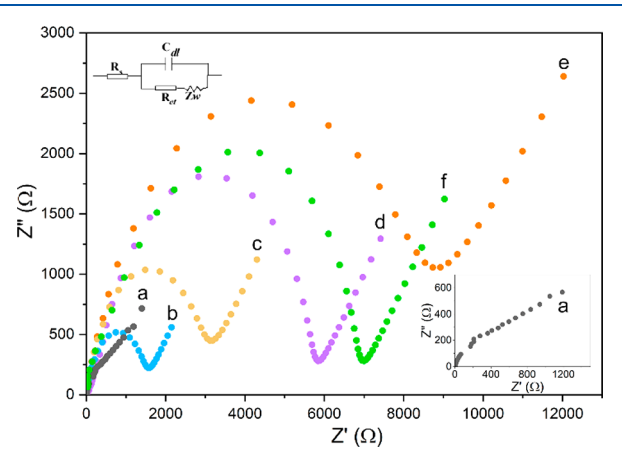


Figure 3. Nyquist plots of impedance spectra at different modification stages of DNA biosensor. Bare gold electrode (a); PDA-modified electrode (b); probe DNA immobilization (c); target DNA hybridization (d); DNA-functionalized AuNP hybridization (e); and CNT-AuNP nanocomposites hybridization (f).

the target DNA dropped onto the biosensor surface, the R_{ct} value further increased from 3500 Ω to 6000 Ω , indicating that the target DNA could be recognized by the constructed biosensor via hybridization. This led to a further increase in the electron-transfer resistance between [Fe(CN)₆]^{3-/4-} and the biosensor. Upon introduction of the AuNP/DNA (reporter and linker) conjugates onto the biosensor surface, the R_{ct} value remarkably increased from 6000 Ω to 9800 Ω . This suggested that the AuNP/DNA (reporter and linker) conjugates could be successfully bound to the biosensor surface through hybridization between the target and linker DNA. Eventually, when the DNA-modified CNTs were attached on the surface of the AuNP/DNA (reporter and linker) conjugates, forming the 3D radial CNT-AuNP nanocomposites, a decrease in the R_{ct} value was observed. This indicated that the CNTs here played a role as electron transfer mediators by facilitating the electron transfer between the $[Fe(CN)_6]^{3-/4-}$ and the electrode, thereby enhancing the sensitivity of the biosensor.

This observation was similar to the results reported in a previous study, in which the porous structure of CNTs dramatically increased the contact surface area of a redox probe $([Fe(CN)_6]^{3-/4-})$ and the DNA-wrapped CNTs were more

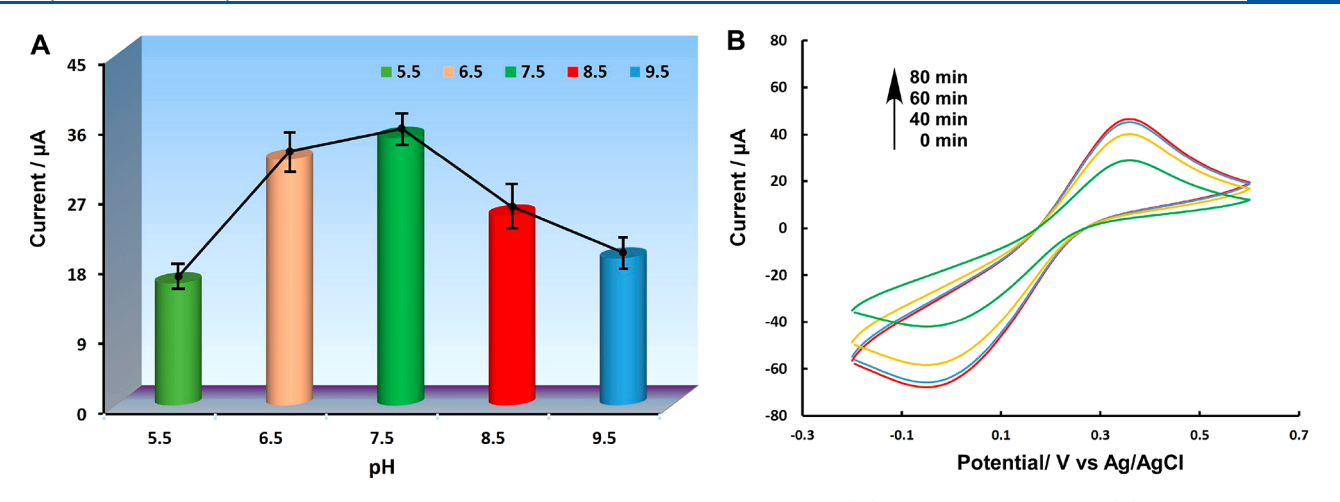


Figure 4. Optimization of the performance of a DNA biosensor. The effects of buffer pH (A) and hybridization time (B) on the peak current.

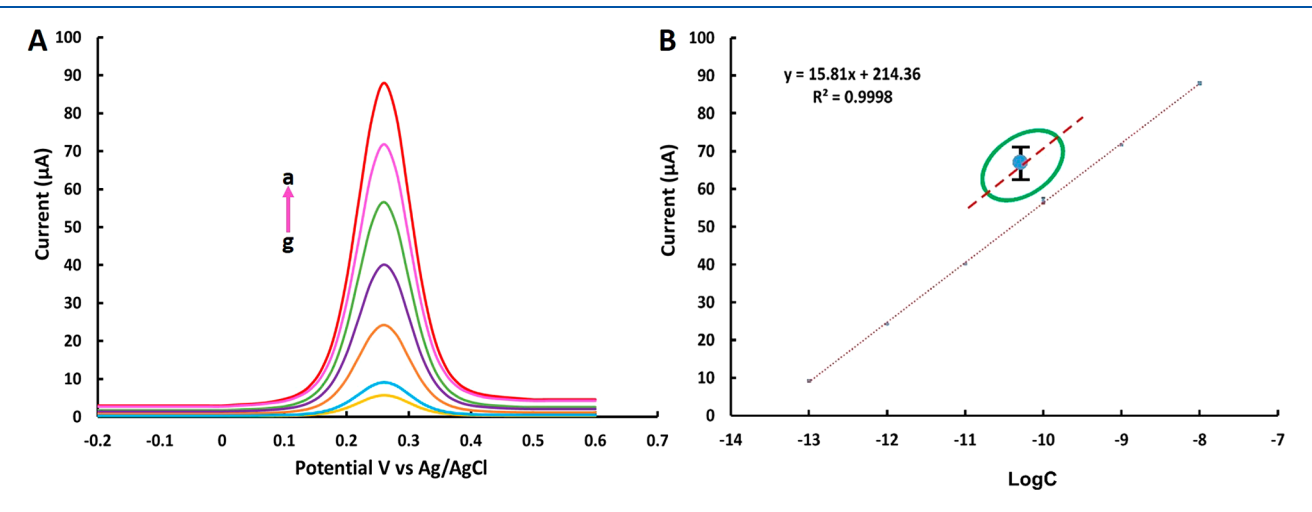


Figure 5. (A) LSV responses of the DNA biosensor to different concentrations of target DNA with the 3D radial AuNP-CNT nanostructures; a: 10 nM, b: 1 nM, c: 100 pM, d: 10 pM, e: 1 pM, and f: 100 fM, g: probe DNA. (B) Linear relationship of current response vs target DNA concentration (n = 3).

Table 1. Comparison of DNA Biosensor Performance with Recent Publications

strategy	analytical technique	linear range	LOD	ref	
MWCNT/AuNPs/Ta	EIS	1.0 fM $-0.1~\mu M$	10 aM	25	
MWCNT/AuNPs	fluorescent	100 fM-1.0 nM	33.4 fM	47	
Au/MNP-CNTs/Pt-IDE	LSV	1.0 pM-10 nM	8.4 pM	48	
GNPs/MWCNTs/gold electrode	DPV	0.01 nM-0.5 nM	7.5 pM	24	
DNA/AuNPs/PABA/MWCNTs/GCE	DPV	1.0 pM-5.0 nM	0.35 pM	49	
Fe2O3/MWCNT/AuNPs	SWV	6 nM-0.3 μM	6 nM	50	
GNPs/SWCNTs/PDA/gold electrode	LSV	0.1 pM-10 nM	5.2 fM	this study	

hydrophilic and easier to contact with the aqueous solution. Those factors are known to be critical for enhancement of electron transfer and improvement of the sensitivity of electrochemical biosensors. In order to confirm that enhancement of the sensitivity of the DNA biosensor was induced by 3D radial CNT-AuNP structures, and not by the physical absorbed CNTs on the surfaces of electrodes, a control experiment was conducted. Instead of using endmodified CNTs, with covalently attached DNA (complementary to reporter DNA on the surface of AuNPs), CNTs were directly incubated with AuNP/DNA bound electrodes. After they were washed, there was no obvious difference in the resistance $R_{\rm ct}$ value, before and after the addition of CNTs (Figure S3), indicating that the decrease in $R_{\rm ct}$ was caused by

the attachment of DNA-modified CNTs on the AuNP surface, and the formation of urchinlike 3D nanoclusters.

Biosensor Optimization. In order to achieve the optimal assay performance of the fabricated biosensor, the effects of pH and hybridization time for the target DNA detection were investigated. As can be seen in Figure 4A, the LSV peak currents increased with increases in pH value, until a pH of 7.5 was reached, and then decreased when the pH increased further. Thus, considering the detection sensitivity, pH 7.5 was chosen as the optimal pH value. Figure 4B shows the dependence of the LSV responses on hybridization time. It was evident that the peak currents increased rapidly, with increasing hybridization time, and remained nearly constant

within 60 min. Therefore, 60 min was employed as the target for DNA detection.

Analytical Performance of a DNA Biosensor. Under optimized experimental conditions, the sensitivity of a fabricated biosensor was investigated with different concentrations of a target DNA. As shown in Figure 5A, the LSV response of the DNA biosensor increased with increases in the target DNA concentrations. A good linear relationship was observed between the peak currents and the logarithm of the concentrations of the target DNA that ranged from 10 nM to 100 fM (Figure 5B). The corresponding regression equation was $I = 15.81\log C_{DNA} + 214.36$ ($R^2 = 0.9998$). The detection limit was estimated to be 5.2 fM, according to the $3\sigma/a$ criterion (where a is the slope of the liner regression, and σ is the standard deviation of the blank analysis), which is much lower than those reported in the literature (AuNP-decorated CNTs-assisted DNA sensing) (Table 1).47-50 A comparison experiment was also performed (Figure S4), which demonstrated the detection limit of the proposed biosensor increased 25 times with and without CNT involvement (Figure S5). This high sensitivity would most likely be related to the structural feature of the 3D radial CNT-AuNP nanocomposites. The radially distributed CNTs around the AuNP core can effectively facilitate the electron transfer rate and, thereby, improve the sensing performance.

Selectivity of Biosensor. The selectivity of the fabricated biosensor was evaluated by testing its LSV responses after hybridization with complementary, single-base-mismatched, two-base-mismatched, and noncomplementary DNA sequences, respectively. It can be seen from Figure 6 that the

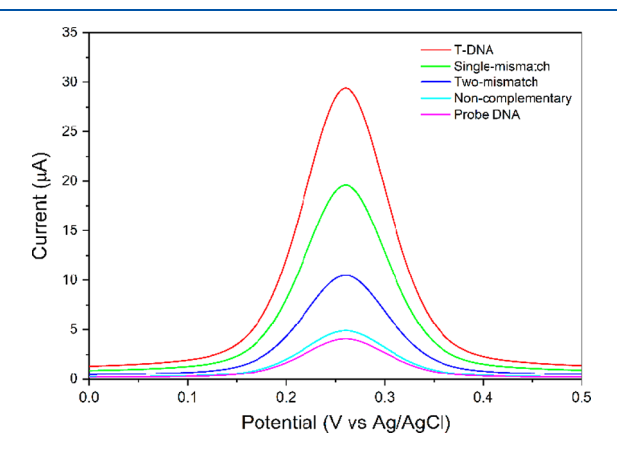


Figure 6. (A) LSV responses of the DNA biosensor for the probe DNA, single-base mismatched sequences, two-base mismatched sequences, noncomplementary DNA, and target DNA (DNA concentration is 10 pM).

hybridization of the probe to the target DNA resulted in the strongest signal intensity, as compared with mismatched DNA sequences. As expected, with an increase in the number of mismatches, the LSV signals gradually decreased. Only a

negligible change in the LSV curve was observed in the noncomplementary DNA, when compared with the probe alone. Therefore, these results indicated that the constructed biosensor had good specificity for detection of the target DNA. In addition, increasing the numbers of CNTs attached on the surface of AuNPs will help to further enhance the signal amplification.

Target DNA Analysis in Human Serum. To demonstrate the feasibility of practical application of the proposed biosensor, in this study, human serum was conveniently utilized as real biological samples for target DNA detection. Three concentrations of DNA (1, 10, and 1000 pM) spiked into the human serum (1% and 10%) were tested by the developed biosensor, respectively. The resulting percentage of recovery and relative standard deviation (RSD) were calculated and listed in Table 2. For every concentration of DNA in human serum, the recovery percentages were close to 100% with low RSD, indicating the high accuracy of the DNA biosensor for electrochemical detection in real biological samples.

Regeneration and Stability of the DNA Sensor. The stability and regeneration ability are considered as the important indicators for the practical applications of biosensors. The regeneration of this DNA biosensor was evaluated, which was carried out by treating the hybridized electrode with urea solutions (8 M) for 30 s to break the DNA duplexes and subsequently rinsed with DI water and then applied again for the analysis of 10 pM target DNA sample. The results indicated that the proposed biosensor could be repeatedly used for assembly disassembly cycles for 5 times with a slight signal decreasing (Figure 7). Storage of the

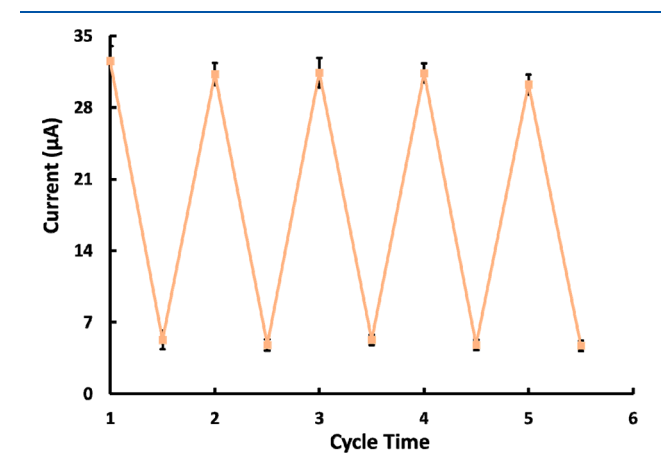


Figure 7. Reversible changes of the extinction peak currents for the biosensor during five cycles of disassembly and assembly processes (target DNA concentration 10 pM).

modified electrode in PBS buffer under 4 $^{\circ}$ C for 5 days resulted in a change of 6.15% signal attenuation in LSV response. Overall, this urchinlike CNT-AuNP-assisted DNA

Table 2. Recovery Detection of Target DNA in Human Serum with the Proposed Biosensor (n = 3)

		1% human serum			10% human serum			
sample	target DNA added (pM)	target DNA detected (pM)	RSD (%)	recovery (%)	target DNA detected (pM)	RSD (%)	recovery (%)	
1	1	1.01, 1.07, 0.98	2.67	99.0	1.03, 0.96, 1.12	7.74	103.7	
2	10	9.93, 9.77, 10.23	2.34	99.8	9.75, 10.34, 9.88	3.10	99.9	
3	1000	1013.27, 989.76, 998.65	1.19	100.1	1013.33, 996.28, 1032.41	1.78	101.4	

biosensor exhibited a good stability and regeneration capability.

CONCLUSIONS

In summary, we have fabricated a sensitive and label-free electrochemical DNA biosensor for sequence-specific DNA detection, based on the "urchinlike" 3D radial AuNP-CNT nanocomposites. Electropolymerization of PDA film on an electrode provided a stable, biocompatible, and functional reactive layer to immobilize DNA probes in a highly dense fashion. In addition, the synergistic properties of 3D radial CNT-AuNP nanostructures significantly enhanced the performance of the DNA biosensor with signal amplification. The constructed biosensor could reach the detection limit of a target DNA as low as 5.2 fM and exhibited good selectivity for distinguishing mismatched DNA sequences and noncomplementary sequences under optimal conditions, as well as excellent stability and regeneration ability. This suggested that the 3D radial CNT-AuNP nanocluster-based biosensor offered potential opportunities for sensitive and accurate detection of DNA for medical diagnosis and applications in many other fields.

ASSOCIATED CONTENT

Supporting Information

The Supporting Information is available free of charge at https://pubs.acs.org/doi/10.1021/acs.analchem.9b03520.

DNA sequences, length distribution of CNTs, and control experiments (PDF)

AUTHOR INFORMATION

Corresponding Authors

Wenyan Liu — Department of Chemistry and Center for Research in Energy and Environment, Missouri University of Science and Technology, Rolla, Missouri 65409, United States; Email: liuweny@mst.edu

Risheng Wang — Department of Chemistry, Missouri University of Science and Technology, Rolla, Missouri 65409, United States; orcid.org/0000-0001-6539-1565; Email: wangri@mst.edu

Authors

Shuo Han — Department of Chemistry, Missouri University of Science and Technology, Rolla, Missouri 65409, United States Ming Zheng — Materials Science and Engineering Division, National Institute of Standards and Technology, Gaithersburg, Maryland 20899, United States; □ orcid.org/0000-0002-8058-1348

Complete contact information is available at: https://pubs.acs.org/10.1021/acs.analchem.9b03520

Author Contributions

The manuscript was written through contributions of all authors. All authors have given approval to the final version of the manuscript.

Notes

The authors declare no competing financial interest.

■ ACKNOWLEDGMENTS

This work was supported by the National Science Foundation under grants CCF-1814797, and Center for Biomedical Research of Missouri S&T.

REFERENCES

- (1) Liu, X.; Tan, W. Anal. Chem. 1999, 71, 5054-5059.
- (2) Ecker, D. J.; Sampath, R.; Massire, C.; Blyn, L. B.; Hall, T. A.; Eshoo, M. W.; Hofstadler, S. A. *Nat. Rev. Microbiol.* **2008**, *6*, 553–558
- (3) Meng, H. M.; Liu, H.; Kuai, H.; Peng, R.; Mo, L.; Zhang, X. B. Chem. Soc. Rev. **2016**, 45, 2583–2602.
- (4) Cinti, S.; Proietti, E.; Casotto, F.; Moscone, D.; Arduini, F. Anal. Chem. 2018, 90, 13680–13686.
- (5) Bohme, K.; Calo-Mata, P.; Barros-Velazquez, J.; Ortea, I. J. Agric. Food Chem. **2019**, 67, 3854–3864.
- (6) Wang, T.; Zhou, L.; Bai, S.; Zhang, Z.; Li, J.; Jing, X.; Xie, G. Biosens. Bioelectron. 2016, 78, 464–470.
- (7) Kim, J.; Campbell, A. S.; de Avila, B. E.; Wang, J. Nat. Biotechnol. **2019**, *37*, 389–406.
- (8) Rogers, K. R.; Gerlach, C. L. Environ. Sci. Technol. 1996, 30, 486A-491A.
- (9) Drummond, T. G.; Hill, M. G.; Barton, J. K. Nat. Biotechnol. 2003, 21, 1192-1199.
- (10) Cheng, Y.; Zhang, X.; Li, Z.; Jiao, X.; Wang, Y.; Zhang, Y. Angew. Chem., Int. Ed. 2009, 48, 3268-3272.
- (11) Zhang, P.; Wu, X.; Yuan, R.; Chai, Y. Anal. Chem. 2015, 87, 3202-3207.
- (12) Chen, Y.; Jiang, B.; Xiang, Y.; Chai, Y.; Yuan, R. Chem. Commun. 2011, 47, 12798–12800.
- (13) Bao, J.; Hou, C.; Zhao, Y.; Geng, X.; Samalo, M.; Yang, H.; Bian, M.; Huo, D. *Talanta* **2019**, *196*, 329–336.
- (14) Zang, Y.; Lei, J.; Ling, P.; Ju, H. Anal. Chem. 2015, 87, 5430–5436.
- (15) Chu, Y.; Deng, A. P.; Wang, W.; Zhu, J. Anal. Chem. 2019, 91, 3619–3627.
- (16) Wang, J.; Li, J.; Baca, A. J.; Hu, J.; Zhou, F.; Yan, W.; Pang, D. W. Anal. Chem. **2003**, 75, 3941–3945.
- (17) Zhu, D.; Liu, W.; Zhao, D.; Hao, Q.; Li, J.; Huang, J.; Shi, J.; Chao, J.; Su, S.; Wang, L. ACS Appl. Mater. Interfaces 2017, 9, 35597–35603
- (18) Zhao, W.; Lam, J. C.; Chiuman, W.; Brook, M. A.; Li, Y. Small **2008**, 4, 810–816.
- (19) Guo, S.; Wang, E. Anal. Chim. Acta 2007, 598, 181-192.
- (20) Campbell, C. N.; Gal, D.; Cristler, N.; Banditrat, C.; Heller, A. Anal. Chem. 2002, 74, 158–162.
- (21) Zribi, B.; Roy, E.; Pallandre, A.; Chebil, S.; Koubaa, M.; Mejri, N.; Magdinier Gomez, H.; Sola, C.; Korri-Youssoufi, H.; Haghiri-Gosnet, A. M. *Biomicrofluidics* **2016**, *10*, 014115.
- (22) Wang, J.; Liu, G.; Jan, M. R. J. Am. Chem. Soc. 2004, 126, 3010-3011.
- (23) Tang, X.; Bansaruntip, S.; Nakayama, N.; Yenilmez, E.; Chang, Y. L.; Wang, Q. *Nano Lett.* **2006**, *6*, 1632–1636.
- (24) Ma, H.; Zhang, L.; Pan, Y.; Zhang, K.; Zhang, Y. Electroanalysis **2008**, 20, 1220–1226.
- (25) Fayazfar, H.; Afshar, A.; Dolati, M.; Dolati, A. Anal. Chim. Acta 2014, 836, 34–44.
- (26) Huang, N.; Zhang, S.; Yang, L.; Liu, M.; Li, H.; Zhang, Y.; Yao, S. ACS Appl. Mater. Interfaces 2015, 7, 17935–17946.
- (27) Chen, K. J.; Wang, C. H.; Liao, C. W.; Lee, C. K. Int. J. Biol. Macromol. 2018, 120, 325-331.
- (28) Shen, J.; Zhang, R.; Su, Y.; Shi, B.; You, X.; Guo, W.; Ma, Y.; Yuan, J.; Wang, F.; Jiang, Z. J. Mater. Chem. A 2019, 7, 18063—18071.
- (29) Ryu, J. H.; Messersmith, P. B.; Lee, H. ACS Appl. Mater. Interfaces 2018, 10, 7523-7540.
- (30) Wang, R.; Bowling, I.; Liu, W. RSC Adv. 2017, 7, 3676-3679.
- (31) Zheng, M.; Jagota, A.; Semke, E. D.; Diner, B. A.; Mclean, R. S.; Lustig, S. R.; Richardson, R. E.; Tassi, N. G. *Nat. Mater.* **2003**, 2, 338–342.
- (32) Ao, G.; Streit, J. K.; Fagan, J. A.; Zheng, M. J. Am. Chem. Soc. **2016**, 138, 16677–16685.
- (33) Streit, J. K.; Fagan, J. A.; Zheng, M. Anal. Chem. **2017**, 89, 10496–10503.

- (34) Penzo, E.; Palma, M.; Wang, R.; Cai, H.; Zheng, M.; Wind, S. J. *Nano Lett.* **2015**, *15*, 6547–6552.
- (35) Wang, J. L.; Li, B. C.; Li, Z. J.; Ren, K. F.; Jin, L. J.; Zhang, S. M.; Chang, H.; Sun, Y. X.; Ji, J. *Biomaterials* **2014**, *35*, 7679–7689.
- (36) Cai, J.; Huang, J.; Ge, M.; Iocozzia, J.; Lin, Z.; Zhang, K. Q.; Lai, Y. Small **2017**, 13, 1604240.
- (37) Li, S.; Wang, H.; Young, M.; Xu, F.; Cheng, G.; Cong, H. Langmuir 2019, 35, 1119–1125.
- (38) Lee, H.; Dellatore, S. M.; Miller, W. M.; Messersmith, P. B. Science 2007, 318, 426-430.
- (39) Lane, R. F.; Hubbard, A. T. Anal. Chem. 1976, 48, 1287-1283.
- (40) Hawley, M. D.; Tatawawadi, S. V.; Piekarski, S.; Adams, R. N. J. Am. Chem. Soc. **196**7, 89, 447–450.
- (41) Eissa, S.; Zourob, M. Anal. Chem. 2017, 89, 3138-3145.
- (42) Gu, H.; Su, X.; Loh, K. P. J. Phys. Chem. B 2005, 109, 13611–13618.
- (43) Napier, M. E.; Hull, D. O.; Thorp, H. H. J. Am. Chem. Soc. 2005, 127, 11952–11953.
- (44) Liu, S.; Lin, B.; Yang, X.; Zhang, Q. J. Phys. Chem. B 2007, 111, 1182–1188.
- (45) Long, R.; Prezhdo, O. V. Nano Lett. 2014, 14, 3335-3341.
- (46) Yu, J.; Zvarec, O.; Huang, D. M.; Bissett, M. A.; Scanlon, D. B.; Shapter, J. G.; Abell, A. D. Chem. Commun. 2012, 48, 1132–1134.
- (47) Ma, H.; Xue, N.; Li, Z.; Xing, K.; Miao, X. Sens. Actuators, B 2018, 266, 221-227.
- (48) Lee, J.; Morita, M.; Takemura, K.; Park, E. Y. Biosens. Bioelectron. 2018, 102, 425-431.
- (49) Zhang, Y.; Wang, J.; Xu, M. Colloids Surf., B 2010, 75, 179-185
- (50) Sumathi, C.; Muthukumaran, P.; Radhakrishnan, S.; Ravi, G.; Wilson, J. RSC Adv. **2015**, *5*, 17888–17896.